Native defects in tetradymite $Bi_2(Te_xSe_{3-x})$ topological insulators

Lin-Lin Wang,[1,*] Mianliang Huang,[2] Srinivasa Thimmaiah,[1] Aftab Alam,[1] Sergey L. Bud'ko,[1] Adam Kaminski,[1,3] Thomas A. Lograsso,[1] Paul Canfield,[1,3] and Duane D. Johnson[1,4,†]

[1]*Division of Materials Science and Engineering, Ames Laboratory, Ames, Iowa 50011, USA*

[2]*Materials and Metallurgical Engineering Department, South Dakota School of Mines, Rapid City, South Dakota 57701, USA*

[3]*Department of Physics and Astronomy, Iowa State University, Ames, Iowa 50011, USA*

[4]*Department of Materials Science and Engineering, Iowa State University, Ames, Iowa 50011, USA*

(Received 23 April 2012; revised manuscript received 18 February 2013; published 8 March 2013)

Formation energies of native defects in $Bi_2(Te_xSe_{3-x})$, with comparison to ideal Bi_2Te_2S, are calculated in density-functional theory to assess transport properties. Bi_2Se_3 is found to be n type for both Bi- and Se-rich growth conditions, while Bi_2Te_3 changes from n to p type going from Te- to Bi-rich conditions, as observed. Bi_2Te_2Se and Bi_2Te_2S are generally n type, explaining observed heavily doped n-type behavior in most samples. A $(0/-)$ transition level at 16 meV above valence-band maximum for Bi on Te antisites in Bi_2Te_2Se is related to the observed thermally active transport gap causing a p-to-n transition at low temperature. $Bi_2(Te_xSe_{3-x})$ with $x > 2$ are predicted to have high bulk resistivity due to effective carrier compensation when approaching the n-to-p crossover. Predicted behaviors are confirmed from characterization of our grown single crystals.

DOI: 10.1103/PhysRevB.87.125303 PACS number(s): 73.43.−f, 72.25.Hg, 73.20.−r, 85.75.−d

I. INTRODUCTION

Binary tetradymites, Bi_2Se_3 and Bi_2Te_3, have been regarded as prototype three-dimensional (3D) topological insulators (TIs).[1,2] Tetradymites have a quintuple-layer structure ($R\bar{3}m$) formed by group V and VI elements, i.e., VI^{I}-V-VI^{II}-V-VI^{I}, with van der Waals interaction between the quintuple layers, making the VI^{I} layer the cleavage plane with the operative surface band structure.[3] Reflecting Hume-Rothery's size and electronegative rules, Bi_2Se_3 and Bi_2Te_3 form a continuous solid solution at the two nonequivalent group-VI sites, with the smaller (more electronegative) Se preferring the inner VI^{II} site and the larger (more electropositive) Te preferring the outer VI^{I} site.[4–6] In such materials, due to spin-orbit coupling, a metallic surface state forms a Dirac cone in the bulk band gap and is protected by time-reversal symmetry against backscattering from nonmagnetic impurities. Ternary tetradymites $Bi_2(Te_xSe_{3-x})$ and Bi_2Te_2S are also 3D TIs and their band structures have been studied showing that the Dirac cone can be tuned by layer chemistry.[3,7–10]

While offering tremendous opportunities for controllable, low-resistance spintronics devices, the transport properties of tetradymites are critical and are affected by layer chemistry, which controls the location of the Dirac cone and alters the stability of native/intrinsic defects. Here, we detail the operative native defects in tetradymites and show how chemistry impacts their behavior with a direct comparison to experiments, including our as-grown ternary samples.

Native defects of low formation energy, such as, doubly charged Se vacancies, $V_{Se^I}^{2+}$ act as donors, whereas singly charged Bi antisites $Bi_{Te^I}^{-}$ act as acceptors. Thus, Bi_2Se_3 and Bi_2Te_3 easily become heavily doped, exhibiting near metallic conductivity,[11,12] and bulk conductance overwhelms the surface contribution. However, the local defect concentration is hard to control and depends sensitively on growth method and condition. To find a semiconducting sample, one often needs to peel off many samples from as-grown crystals.[13,14]

Recently, groups have explored $Bi_2(Te_xSe_{3-x})$ attempting to grow 3D TIs with high bulk resistivity needed for device operation. Ren *et al.*[15] have grown $Bi_2Te_{1.95}Se_{1.05}$ crystals at 850 °C that show a bulk resistivity above 1 Ω cm, and observed a p-to-n type transition at ∼100 K; these results were interpreted as a shallow acceptor level at 30 meV above valence-band maximum (VBM). In another study, Ren *et al.*[16] also found that a sample grown at $x = 2.1$ also shows high bulk resistivity. Xiong *et al.*[17] have shown that the bulk resistivity of Bi_2Te_2Se can reach as high as 6 Ω cm. Using different growth methods, Jia *et al.*[18] observed that most Bi_2Te_2Se samples have low resistivity and a heavily doped *n-type* (not p-type) behavior. Only some samples grown at $2:2:(1-x)$ give high resistivity and also show a p-to-n-type transition at low temperature (T). Luo *et al.*[19] found that this transport gap is sensitive to hydrostatic pressure and measured a 50-meV activation energy. But the origin of such an acceptor level is still unknown.

To understand bulk transport behavior of $Bi_2(Te_xSe_{3-x})$, we use density-functional theory[20,21] (DFT) to study the thermodynamics of native defects in these materials.[22] DFT studies of the neutral defects in Bi_2Te_3 found that antisites Bi_{Te^I} and Te_{Bi} dominate in Bi- and Te-rich conditions, respectively.[23] Native defects in Sb_2Te_3 were calculated without considering the effect of chemical conditions.[24] Recently Scanlon *et al.*[10] studied the native defects in tetradymites and showed that by changing Te content, the Fermi level can be tuned into the band gap. But the formation energy of donor $V_{Se^I}^{2+}$ for Bi_2Se_3 was found to be as high as 1 eV near conduction-band minimum (CBM). Here, from the formation energies of native defects in $Bi_2(Te_xSe_{3-x})$ and Bi_2Te_2S, besides calculating defect concentrations, we identify the majority carrier type to compare with experimental characterization and also study the behaviors in bulk transport properties.

II. COMPUTATIONAL AND EXPERIMENTAL METHODS

To calculate formation energy of native defects, we use the orthorhombic unit cell of tetradymite and construct a $(5 \times 3 \times 1)$ supercell of 450 atoms and use VASP[25,26] with

projector augmented wave method[27] and PW91[28] as exchange correlation functional. A $(2 \times 2 \times 2)$ k-point mesh with a Gaussian smearing of 0.05 eV is used and the absolute values of forces on atoms are relaxed below 0.02 eV/Å. Default kinetic energy cutoffs in VASP (Bi 105 eV, Te 175 eV, Se 212 eV, and S 280 eV) are used to minimize the computational cost for such a large supercell. Because a large part of defect formation energy[22] is calculated as the total-energy difference between two large supercells always having the same energy cutoff, error cancellation ensures good accuracy of the results. Separate calculations with 400-eV cutoff only show a 2-meV difference in defect formation energy. For the crystal phases that determine the atomic chemical potentials, the energies are calculated with 400-eV energy cutoff to ensure good convergence. The defect formation energies are all calculated in theoretical lattice parameters without spin-orbital coupling.

We apply charge neutrality conditions to find the Fermi level (ε_f) pinned from DOS (with "scissor operation" to improve gaps) and contributions from native defects. Because details of the valence- and conduction-band edges affect the pinning of ε_f, bulk density of states (DOS) are calculated in experimental lattice parameters with spin-orbit coupling on a dense k-point mesh of $(18 \times 18 \times 18)$. The calculated (experimental) band gaps from DOS are 0.320 (0.350),[29] 0.097 (0.165),[30] 0.247 (0.300),[15] and 0.274 eV for Bi_2Se_3, Bi_2Te_3, Bi_2Te_2Se, and Bi_2Te_2S, respectively. With no experimental band gap for Bi_2Te_2S, we take the same value as Bi_2Te_2Se.

In experiment, proper ratio of high purity metals of Bi (99.999%), Se (99.999%), and Te (99.999%) were sealed in a quartz tube and melted into an ingot in an induction furnace to homogenize the composition. The ingot was then sealed in a quartz tube with a larger diameter and loaded into a Bridgman furnace. Crystal was obtained by withdrawing the quartz tube at 1 mm/h after being heated to and kept at 800 °C. The concentration profile along the ingot was obtained by using electron probe microanalysis. These gradients in the as-grown ingot result from liquid convection during crystal growth and are associated with the solid solution nature of the phase equilibria in the quasibinary system Bi_2Te_3-Bi_2Se_3. These gradients can be fitted using a fully mixed convective model and the starting compositions adjusted to yield a targeted composition. A thin slab with a desired composition was cut from the ingot to make samples for resistivity measurement. Resistivity measurement was carried out in a Quantum Design physical property measurement system.

III. RESULTS AND DISCUSSION

Figure 1 shows the formation energies of three native defects in the tetradymites as a function of ε_f from VBM to CBM. For Bi_2Se_3 under Se-rich conditions [Fig. 1(a) bottom panel], due to the low chemical potential of Se, a singly charged Se on Bi antisite, Se^{+}_{Bi}, has the lowest formation energy and acts a shallow donor. Close in energy is the doubly charged vacancy on Se^{I} site, $V^{2+}_{Se^I}$, also acting as a shallow donor. With a high Bi chemical potential, Bi on Se^{I} antisite has a much higher energy and changes from a triple donor to a single acceptor at VBM + 0.26 eV. With the charge state of $(3+)$, Bi_{Se^I} has a large relaxation with Bi rising 1.4 Å above the atomic plane

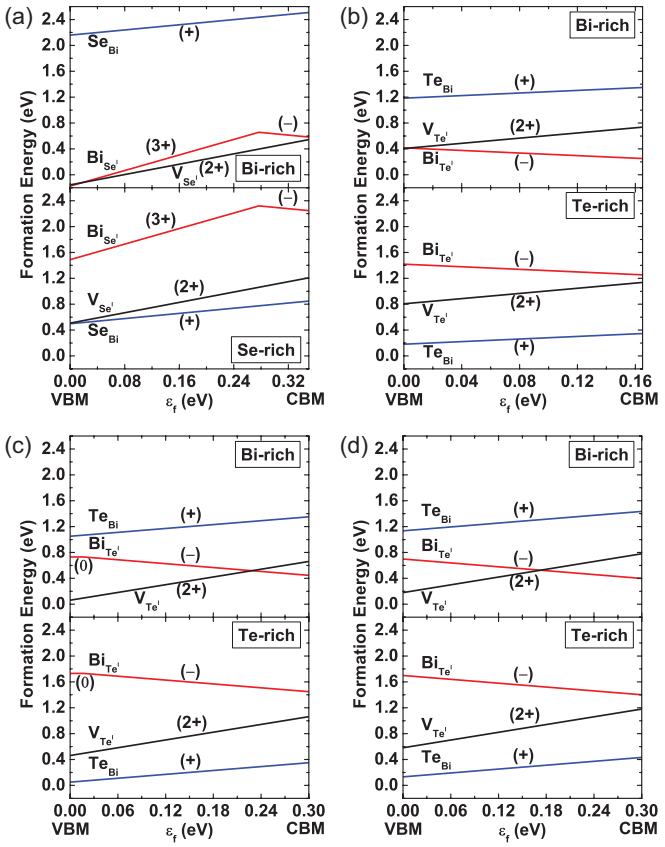

FIG. 1. (Color online) Defect formation energy as a function of ε_f in (a) Bi_2Se_3, (b) Bi_2Te_3, (c) Bi_2Te_2Se, and (d) Bi_2Te_2S. Top (bottom) panel is for Bi- (Se/Te-)rich condition.

(rumpling), showing a strong negative-U behavior, thus $Bi^{3+}_{Se^I}$ is a deep donor. In (−), there is much less relaxation and $Bi^{-}_{Se^I}$ acts as a shallow acceptor. Under Se-rich condition, Bi_2Se_3 behaves as n type because the shallow donor Se^{+}_{Bi} is dominant throughout the band gap.

As the growth condition changes from Se rich to Bi rich [Fig. 1(a) top panel], the chemical potential of Bi decreases to that of Bi crystal and the chemical potential of Se increases. Although the preferred charge state of each defect does not change, the relative stability of the defects changes. Under Bi-rich conditions, Bi is more favorable than Se to enter the compound and similarly Se is more favorable to be pushed out of the compound. Thus, the Se^{+}_{Bi} antisite now has a much higher formation energy than the other two defects, among which $V^{2+}_{Se^I}$ has the lowest throughout the gap, about 0.4 eV at CBM, less than half of what was found by Scanlon *et al.*[10] The main difference is due to that the experimental lattice constants were used in their supercell calculations, which causes the undesirable effect of long-range elastic energy.[22] Although $Bi^{3+}_{Se^I}$ has a low formation energy, close to $V^{2+}_{Se^I}$, it does not contribute to the n-type carrier because it is a deep donor. So, under Bi-rich conditions, Bi_2Se_3 remains n type because the dominant defect $V^{2+}_{Se^I}$ is a double donor.

Our calculations reveal that Bi_2Se_3 stays as n type regardless of chemical conditions, agreeing well with observation that as-grown Bi_2Se_3 is always n type.[11] The reason is that

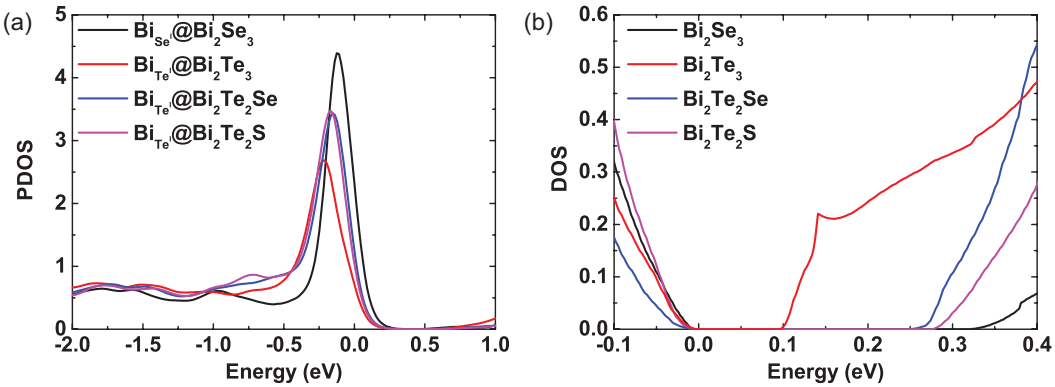

FIG. 2. (Color online) DOS (a) projected on Bi^0_{Se/Te^I} and (b) around band gap for the four tetradymites.

the formation energy of $V^{2+}_{Se^I}$ is very low, especially under Bi-rich conditions, a common scenario when the compound is synthesized at high T, where Se is prone to form Se dimers and leave as vapor. The low formation energy corresponds to observed high concentration of $V^{2+}_{Se^I}$.

For Bi_2Te_3 under Te-rich conditions [Fig. 1(b) bottom panel], Te^+_{Bi} antisite like Se^+_{Bi} in Bi_2Se_3, has the lowest formation energy and acts as a shallow donor. The other two native defects, $V^{2+}_{Te^I}$ and $Bi^-_{Te^I}$, have higher formation energy. Unlike Bi_{Se^I} in Bi_2Se_3, Bi_{Te^I} in Bi_2Te_3 acts as a shallow acceptor in $(-)$, because it costs a much higher energy to empty the three electrons in the Bi_{Te^I}-derived levels than Bi_{Se^I} due to the less ionic bonding. Because of the low formation energy of Te^+_{Bi} for Te-rich conditions, Bi_2Te_3 behaves as n type. For Bi_2Te_3 under Bi-rich conditions [Fig. 1(b) top panel], Te^+_{Bi} is pushed higher in energy due to the changes in chemical potential and it becomes irrelevant in determining carrier type, while $Bi^-_{Te^I}$ becomes much more stable with a large drop in the formation energy, bringing it even lower than $V^{2+}_{Te^I}$. As a result, $Bi^-_{Te^I}$, a singly charged acceptor, becomes the dominant defect, with a formation energy of 0.42 eV at VBM. Thus, under Bi-rich conditions, Bi_2Te_3 behaves as p type instead of n type.

In contrast to Bi_2Se_3, which is n type under both Se- and Bi-rich conditions, Bi_2Te_3 changes from n type to p type from Te- to Bi-rich conditions. This agrees well with a recent molecular-beam epitaxy experiment[31] on Bi_2Te_3, where a n- to p-type transition was observed by increasing the substrate's temperature. As the growth temperature increases, Te atoms are more likely to form Te-dimer vapor, leaving the system Bi rich and favoring the formation of $Bi^-_{Te^I}$, which changes the majority carrier from n to p type.

For ternaries under Te-rich conditions, see bottom panels of Figs. 1(c) and 1(d), the trend in stability of defects in Bi_2Te_2Se and Bi_2Te_2S are similar to those in Bi_2Te_3, with the Te^+_{Bi} lowest, followed by $V^{2+}_{Te^I}$ donor, and the $Bi^-_{Te^I}$ acceptor highest. Again, for Te-rich conditions, Bi_2Te_2Se and Bi_2Te_2S should behave as n type because of the dominant Te^+_{Bi} shallow donor. Compared to Bi_2Te_3, the formation energies of $V^{2+}_{Te^I}$ and Te^+_{Bi} decrease in Bi_2Te_2Se and Bi_2Te_2S, while that of the $Bi^-_{Te^I}$ increases, as seen under Bi-rich conditions [Figs. 1(c) and 1(d) top panels]. In contrast to no crossing of defect levels in Bi_2Te_3, $V^{2+}_{Te^I}$ and $Bi^-_{Te^I}$ do cross in the gap for Bi-rich Bi_2Te_2Se and Bi_2Te_2S (due to the increase of formation energy for $Bi^-_{Te^I}$ and the decrease for $V^{2+}_{Te^I}$). Particularly, for $Bi^-_{Te^I}$ in Bi_2Te_2Se, there is a transition level of $(0/-)$ at VBM + 16 meV.

DOS projected on Bi antisite are plotted in Fig. 2(a). Compared to the most ionic compound Bi_2Se_3, where Bi induces a sharp peak as the impurity level at the top of the valence band, the same peak is more broadened and shifts toward lower energy in the least ionic compound Bi_2Te_3. Those for Bi_2Te_2Se and Bi_2Te_2S are in between, explaining why the formation energy for Bi antisite is the lowest in Bi_2Te_3 and highest in Bi_2Se_3. Between the two nonequivalent group-VI sites, VI^{II} is more ionically and strongly bonded than VI^{I}. So, the vacancy and antisite on the VI^{I} site have lower formation energy than those on the VI^{II} site. Even for Bi_2Te_2Se, we find that $V^{2+}_{Te^I}$ has a lower formation energy than $V^{2+}_{Se^{II}}$.

Total DOS determines the chemical stability and defect formation energy. However, transport properties and the intrinsic Fermi level (ε^I_f) are more directly related to the DOS around band edges [Fig. 2(b)]. Whether a material has n- or p-type majority carriers is determined by the position of the defect-pinned Fermi level (ε^D_f) relative to ε^I_f, established solely by DOS. Both Fermi levels are calculated from charge neutral conditions and are shown in Fig. 3 as a function of temperature.

For Bi_2Se_3, because the valence-band edge (VBE) has more DOS and rises faster than the conduction-band edge (CBE), see Fig. 2(b), ε_f must be in the upper half of the band gap to have an equal concentration of electrons and holes. The ε^I_f reflects directly the shapes of the band edges; see Fig. 3(a). For Bi_2Te_3, VBE has slightly less DOS from 0.1 to 0.15 eV then rises faster than CBE. So, ε^I_f first decreases, levels off, and then increases beyond 400 K. For ternaries, the band edges of Bi_2Te_2Se are like Bi_2Te_3 and Bi_2Te_2S is like Bi_2Se_3; see Fig. 2(b). So, ε^I_f in Bi_2Te_2Se first decreases then increases as T increases. For Bi_2Te_2S, ε^I_f increases as T increases, but slower than Bi_2Se_3.

At high T, the contribution from native defects becomes significant in pinning ε_f. For Bi-rich Bi_2Se_3 with dominant $V^{2+}_{Se^I}$, a donor with a low formation energy, ε^D_f is pinned well above ε^I_f, confirming that Bi-rich Bi_2Se_3 is n type. In contrast, for Bi-rich Bi_2Te_3, the dominant $Bi^-_{Te^I}$ acceptor pins ε^D_f nearer VBM even though DOS contribution favors nearer CBM beyond 600 K. The overall effect is that ε^D_f is always

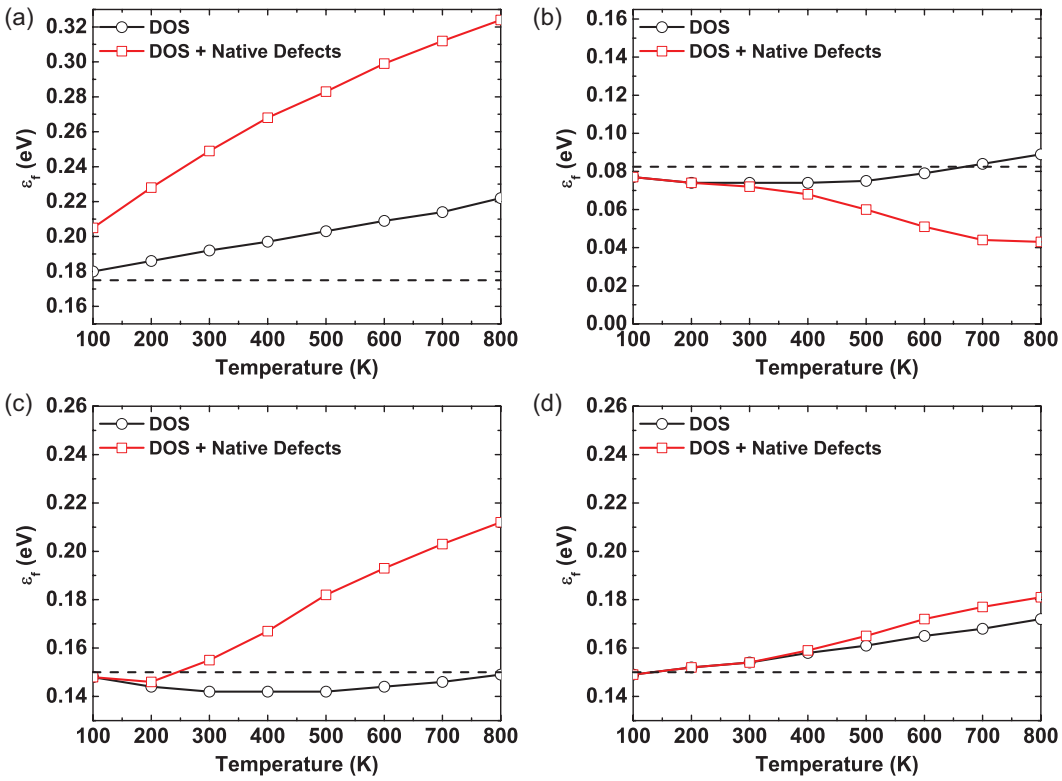

FIG. 3. (Color online) ε_f^I and ε_f^D versus temperature for (a) Bi_2Se_3, (b) Bi_2Te_3, (c) Bi_2Te_2Se, and (d) Bi_2Te_2S under Bi-rich conditions. The dashed line corresponds to the middle of band gap.

pinned below ε_f^I and Bi_2Te_3 behaves as *p* type under Bi-rich conditions. For Bi_2Te_2Se, the combined effects of the native defects of $V_{Te^I}^{2+}$ and $Bi_{Te^I}^{-}$ pin ε_f^D above ε_f^I and thus intrinsically Bi_2Te_2Se is *n* type, not *p* type. At 800 K, ε_f^D is pinned at VBM + 0.21 eV, very close to the crossing point of the formation energies of $V_{Te^I}^{2+}$ and $Bi_{Te^I}^{-}$ at VBM + 0.22 eV. For Bi_2Te_2S, ε_f^D follows closely with and only slightly above ε_f^I. At 800 K, ε_f^D is at VBM + 0.18 eV, reflecting that the formation energies of $V_{Te^I}^{2+}$ and $Bi_{Te^I}^{-}$ cross at the middle of the band gap. So Bi_2Te_2S is only a weak *n* type.

With charge neutrality conditions, defect and carrier concentrations can also be calculated. Table I lists the concentrations of the two native defects with lowest formation energies at 700 K under Bi-rich conditions. For the two binaries, the experimental estimates are also included in parentheses. For Bi_2Se_3, the defects of $V_{Se^I}^{2+}$ and $Bi_{Te^I}^{-}$ have the concentration of 6.1 and 0.5×10^{18} cm^{-3}, respectively, versus 13.0 and 1.1×10^{18} cm^{-3} from experimental estimates.[32] For Bi_2Te_3, the concentrations are 3.2 and 24.5×10^{18} cm^{-3} versus experimental estimates[32] of 4.6 and 17×10^{18} cm^{-3}. Our DFT estimates compare reasonably with those from experiment, especially given the idealized theory scenario used.

TABLE I. Calculated concentrations of native defects V_{Se/Te^I}^{2+} and Bi_{Se/Te^I}^{-} at 700 K under Bi-rich conditions. The experimental estimates in parentheses are from Ref. 32.

$\times 10^{18}$ (cm^{-3})	V_{Se/Te^I}^{2+}	Bi_{Se/Te^I}^{-}
Bi_2Se_3	6.1 (13.0)	0.5 (1.1)
Bi_2Te_3	3.2 (4.6)	24.5 (17.0)
Bi_2Te_2Se	5.3	1.5
Bi_2Te_2S	1.7	2.2

Compared to Bi_2Se_3, the drop in donor defect concentration for Bi_2Te_2Se corresponds to the drop in electron carrier concentration. The dominant defect in Bi_2Te_2Se is still $V_{Te^I}^{2+}$, but the concentration is lowered because of the increased formation energy. For Bi_2Te_2S, the donor defect $V_{Te^I}^{2+}$ formation energy is increased further and results in an even smaller concentration of donor defects, and it becomes comparable to that of the acceptor $Bi_{Te^I}^{-}$. This corresponds to the pinning of ε_f right in the middle of the band gap as seen in Fig. 3(d). So the ternaries should have larger resistivity than binary end points Bi_2Se_3 and Bi_2Te_3. We also predict that ideal Bi_2Te_2S has a higher bulk resistivity than Bi_2Te_2Se.

Our calculated native defect formation energies agree well with the recent measurement by Jia *et al.*[18] that the nominal Bi_2Te_2Se is *n* type, not *p* type. However, the concentrations of native defects are largely affected by growth methods and conditions, where thermodynamic equilibrium is not necessarily reached, causing inhomogeneous defect concentration with a slight off-stoichiometry. Under some conditions, if the formation of $V_{Te^I}^{2+}$ is inhibited or transformed into $Bi_{Te^I}^{-}$, Bi_2Te_2Se can behave like *p*-type and the calculated thermodynamic transition level of $Bi_{Te^I}^{-}$ at VBM + 16 meV correlates well with the transport gap measured in experiments.[15,18]

Bounded by the stoichiometric *n*-type Bi_2Te_2Se and *p*-type Bi_2Te_3 on the two ends under Bi-rich conditions,

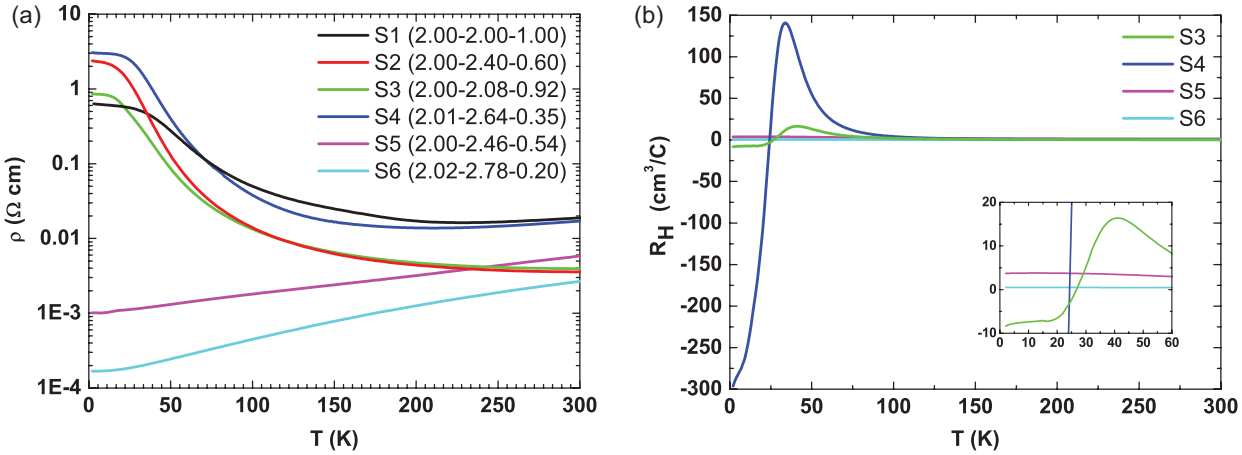

FIG. 4. (Color online) (a) Resistivity and (b) Hall coefficient vs temperature. The compositions of the samples in terms of Bi-Te-Se are included in the parentheses.

the *n-to-p* crossover for $Bi_2(Te_xSe_{3-x})$ when changing only the Te-Se content must be somewhere between $x = 2$ and $x = 3$. The carrier compensation when approaching such a crossover can give high bulk resistivity for $Bi_2(Te_xSe_{3-x})$ with $x > 2$, explained qualitatively by the trends in defect formation energies. For Bi_2Te_2Se, the crossing of $V^{2+}_{Te^I}$ and $Bi^{-}_{Te^I}$ is in the lower half of the band gap, closer to CBM. With increased Te, the crossing moves to the middle of the gap and pins ε_f there, similar to Bi_2Te_2S.

To confirm our predicted transport behaviors, we have grown single crystals of $Bi_2(Te_xSe_{3-x})$ with a continuous variation of x.[6] Among the six samples measured, Fig. 4(a), two (S5 and S6) with high Te content show metallic behavior and are heavily doped p type as revealed by their positive Hall coefficients, which is in contrast to the heavily doped n type that Jia *et al.*[18] found around the stoichiometric Bi_2Te_2Se. The other four samples (S1–S4) show semiconducting behavior with surprisingly high resistivity agreeing with previous studies by Ren *et al.*[16] at $x = 2.1$ and Scanlon *et al.*[10] at $x = 2.5$. Our samples span a wider composition range for Te from $x = 2$ to 2.64 (or 40.0 to 52.7 in at. %), also covering the range of the n-to-p crossover suggested in Seebeck coefficient measurement.[5] The Hall coefficients of S3 and S4 go from positive to negative below 50 K, Fig. 4(b), and can be explained from the calculated thermodynamic transition level of the accepter $Bi^{-}_{Te^I}$ at VBM + 16 meV.

With the assumption of single majority carrier, we get the following results from Hall measurements. For S3 close to 2:2:1 composition, at 10 K, the carrier density is 8.4×10^{17} cm^{-3} and the mobility is 8.9 cm^2/V s. For S4 more Te rich, at 10 K, the carrier density has dropped to 2.4×10^{16} cm^{-3}, the mobility increases to 86 cm^2/V s, due to lower defect densities for higher defect formation energies. The alloying of Te-Se only happens at the Se^{II} layer, while the valence- and conduction-band edges are mostly contributed from the outer two layers of Te and Bi, explaining the small alloying effect on scattering. The small carrier density indicates that the composition is close to the n-to-p crossover, yet the exact crossover point needs further experimental study with careful control of the local defect concentration during sample growth.

IV. CONCLUSION

In conclusion, DFT formation energies of native defects in $Bi_2(Te_xSe_{3-x})$ tetradymites were calculated to study their bulk transport properties. The carrier types were predicted from the identified energetically favored donors and acceptors, explaining the observed (i) heavily doped n-type behavior in Bi_2Te_2Se, (ii) the p-to-n type change in Bi_2Te_3 from Bi- to Te-rich conditions, and (iii) identified (0/−) transition level for $Bi^{-}_{Te^I}$ acceptors in Bi_2Te_2Se that correlates with the observed p-to-n transport gap at low temperature. The predicted high bulk resistivity for $Bi_2(Te_xSe_{3-x})$ with $x > 2$ is confirmed by experiment.

Note added. After completion and submission of this work, we became aware of a related study by West *et al.*[33] on the native defects of the binary tetradymites.

ACKNOWLEDGMENTS

Work at Ames Laboratory was supported by the US Department of Energy, Office of Basic Energy Sciences, Materials Science and Engineering Division. Ames Laboratory is operated for US-DOE by Iowa State University under Contract No. DE-AC02-07CH11358. We thank T. M. Riedemann and W. E. Straszheim for handling and analyzing the sample compositions.

*llw@ameslab.gov
†ddj@ameslab.gov

[1] M. Z. Hasan and C. L. Kane, Rev. Mod. Phys. **82**, 3045 (2010).
[2] X.-L. Qi and S.-C. Zhang, Rev. Mod. Phys. **83**, 1057 (2011).
[3] L.-L. Wang and D. D. Johnson, Phys. Rev. B **83**, 241309(R) (2011).
[4] S. Nakajima, J. Phys. Chem. Solids **24**, 479 (1963).
[5] O. B. Sokolov, S. Y. Skipidarov, N. I. Duvankov, and G. G. Shabunina, J. Cryst. Growth **262**, 442 (2004).

[6]M. Huang, L.-L. Wang, A. Alam, S. Thimmaiah, D. D. Johnson, and T. A. Lograsso (unpublished).
[7]S.-Y. Xu, L. A. Wray, Y. Xia, R. Shankar, A. Petersen, A. Fedorov, H. Lin, A. Bansil, Y. S. Hor, D. Grauer, R. J. Cava, and M. Z. Hasan, arXiv:1007.5111.
[8]R. Jiang, L. L. Wang, M. L. Huang, R. S. Dhaka, D. D. Johnson, T. A. Lograsso, and A. Kaminski, Phys. Rev. B **86**, 085112 (2012).
[9]L. H. Bao, L. He, N. Meyer, X. F. Kou, P. Zhang, Z. G. Chen, A. V. Fedorov, J. Zou, T. M. Riedemann, T. A. Lograsso, K. L. Wang, G. Tuttle, and F. X. Xiu, Sci. Rep. **2**, 726 (2012).
[10]D. O. Scanlon, P. D. C. King, R. P. Singh, A. de la Torre, S. M. Walker, G. Balakrishnan, F. Baumberger, and C. R. A. Catlow, Adv. Mater. **24**, 2154 (2012).
[11]J. G. Checkelsky, Y. S. Hor, M. H. Liu, D. X. Qu, R. J. Cava, and N. P. Ong, Phys. Rev. Lett. **103**, 246601 (2009).
[12]D. X. Qu, Y. S. Hor, J. Xiong, R. J. Cava, and N. P. Ong, Science **329**, 821 (2010).
[13]K. Eto, Z. Ren, A. A. Taskin, K. Segawa, and Y. Ando, Phys. Rev. B **81**, 195309 (2010).
[14]N. P. Butch, K. Kirshenbaum, P. Syers, A. B. Sushkov, G. S. Jenkins, H. D. Drew, and J. Paglione, Phys. Rev. B **81**, 241301(R) (2010).
[15]Z. Ren, A. A. Taskin, S. Sasaki, K. Segawa, and Y. Ando, Phys. Rev. B **82**, 241306(R) (2010).
[16]Z. Ren, A. A. Taskin, S. Sasaki, K. Segawa, and Y. Ando, Phys. Rev. B **84**, 165311 (2011).
[17]J. Xiong, A. C. Petersen, D. X. Qu, Y. S. Hor, R. J. Cava, and N. P. Ong, Physica E **44**, 917 (2012).
[18]S. Jia, H. W. Ji, E. Climent-Pascual, M. K. Fuccillo, M. E. Charles, J. Xiong, N. P. Ong, and R. J. Cava, Phys. Rev. B **84**, 235206 (2011).
[19]Y. Luo, S. Rowley, J. Xiong, S. Jia, R. J. Cava, and N. P. Ong, arXiv:1110.1081.
[20]P. Hohenberg and W. Kohn, Phys. Rev. B **136**, B864 (1964).
[21]W. Kohn and L. J. Sham, Phys. Rev. **140**, 1133 (1965).
[22]C. G. Van de Walle and J. Neugebauer, J. Appl. Phys. **95**, 3851 (2004).
[23]A. Hashibon and C. Elsasser, Phys. Rev. B **84**, 144117 (2011).
[24]T. Thonhauser, G. S. Jeon, G. D. Mahan, and J. O. Sofo, Phys. Rev. B **68**, 205207 (2003).
[25]G. Kresse and J. Furthmuller, Phys. Rev. B **54**, 11169 (1996).
[26]G. Kresse and J. Furthmuller, Comput. Mater. Sci. **6**, 15 (1996).
[27]P. E. Blöchl, Phys. Rev. B **50**, 17953 (1994).
[28]J. P. Perdew and Y. Wang, Phys. Rev. B **45**, 13244 (1992).
[29]J. Black, E. M. Conwell, L. Seigle, and C. W. Spencer, J. Phys. Chem. Solids **2**, 240 (1957).
[30]Y. L. Chen, J. G. Analytis, J. H. Chu, Z. K. Liu, S. K. Mo, X. L. Qi, H. J. Zhang, D. H. Lu, X. Dai, Z. Fang, S. C. Zhang, I. R. Fisher, Z. Hussain, and Z. X. Shen, Science **325**, 178 (2009).
[31]G. Wang, X. G. Zhu, Y. Y. Sun, Y. Y. Li, T. Zhang, J. Wen, X. Chen, K. He, L. L. Wang, X. C. Ma, J. F. Jia, S. B. B. Zhang, and Q. K. Xue, Adv. Mater. **23**, 2929 (2011).
[32]C. Drasar, P. Lostak, and C. Uher, J. Electron. Mater. **39**, 2162 (2010).
[33]D. West, Y. Y. Sun, H. Wang, J. Bang, and S. B. Zhang, Phys. Rev. B **86**, 121201(R) (2012).